Title

Effects of metal cations on corrosion of mild steel in model fresh water

Author Names

Kyohei OTANI[1)], Masatoshi SAKAIRI[2)]

Affiliations

1) Graduate School of Engineering, Hokkaido University, Kita-13, Nishi-8, Kita-ku, Sapporo, Hokkaido 060-8628, Japan

2) Faculty of Engineering, Hokkaido University, Kita-13, Nishi-8, Kita-ku, Sapporo, Hokkaido 060-8628, Japan

Abstract

The effects of metal cations on corrosion of mild steel in model fresh water were investigated by electrochemical techniques and immersion tests. Analysis of X-ray photoelectron spectroscopy showed that metal cations have large hardness of cations, *X*, are incorporated in passive films. The electrochemical and immersion results showed that *X* is not suitable as a corrosion indicator of mild steel. A novel corrosion indicator, "corrosion inhibitory effect of cations *Y*", that consists of *X* and molar volume ratio, ΔV, is proposed, and it is shown that the novel indicator can estimate the corrosion rate of mild steel in fresh water.

Keywords

steel, EIS, SEM, XPS, passive films

Introduction

Corrosion of steel in model fresh water is a serious problem in circulative cooling systems, water supply systems and water storage tanks, and the corrosion has been investigated by many researchers [1-4]. The initial corrosion behaviour of mild steel has been discussed on the basis of passive film structure because the mild steel surface is protected by the passive film in fresh water at the initial stage. There have been many studies on the corrosion of iron and mild steel that focused on chloride ions, and it was shown that chloride ions penetrate through the passive film and then destroy the films [5-9]. After the passive films have been destroyed, the corrosion process of mild steel changes to a coupled electrochemical reaction consisting of anodic metal oxidation (1) and cathodic oxygen reduction (2):

$$Fe(s) = Fe^{2+}(aq) + 2e^{-} \quad (1)$$

$$1/2O_2 + H_2O + 2e^{-} = 2OH^{-} \quad (2)$$

Oxygen reduction requiring water molecules develops in a neutral medium and its reaction current is limited by the oxygen diffusion [10]. The oxidation and reduction steps take place at separate locations on the mild steel [11]. On the other hand, Kato et al. [12] and Takasaki [13] investigated the corrosion behaviour of mild steel by focusing on the effects of metal cations in model fresh water, and they found that zinc ions and aluminium ions have corrosion inhibiting ability. For this reason, the effect of metal cations on the corrosion of mild steel should be considered in fresh water. However, there has been no study in which the quantitative effects of all metal cations on corrosion of mild steel in model fresh water were investigated.

The incorporation of the metal cations into passive films formed on mild steel would be important to clarify the effect of metal cations on the corrosion of mild steel in fresh water, and the HSAB (Hard and Soft Acids and Bases Principle) concept is useful for understanding the incorporation of metal cations. In the HSAB concept, Lewis acids and bases [14] are divided into “hard” and “soft” ions, respectively [15]. Hard acids and hard bases can form stable ionic bonding, and soft acids and soft bases can form stable covalent bonding. Oxygen ions are located on the outermost layer of mild steel, and hard acids are therefore easily incorporated with oxygen ions. However, the incorporation cannot be arranged linearly by the qualitative HSAB concept. The authors focused on “hardness of cations, *X*”, which is an indicator based on the HSAB concept [16]. *X* can explain quantitatively the incorporation between the metal cations and oxygen atoms of the passive films in solution, and the corrosion rate of mild steel may therefore decrease with an increase in *X*. However, the authors previously investigated the effect of metal cations in model fresh water on corrosion rate of an aluminium alloy, and it was found that the corrosion rate of the aluminium alloy could not be explained by *X* of metal cations in the solution [17]. In addition, the layer of metal cations on the passive film of the aluminium alloy was detected by X-ray photoelectron spectroscopy (XPS). It is thought that *X* cannot explain the difference in degrees of protection of metal cation layers, and the corrosion rate of the aluminium alloy was therefore not explained by *X*. It is necessary to investigate the effects of metal cations on corrosion of mild steel that has different passive films from those on the aluminium alloy and to develop a novel indicator that can estimate the corrosion rate of mild steel in fresh water.

In this study, the effects of metal cations on corrosion of mild steel in model fresh water

were investigated by electrochemical impedance spectroscopy (EIS), immersion tests, and surface observation and analysis with SEM and XPS. The different degrees of protection of metal cation layers were explained by the results of these tests and analysis, and the novel indicator which include both the protection and hardness of cations, *X*, was developed.

Materials and methods

Specimens

Mild steel sheets (0.7 mm in thickness) were used as specimens. The chemical composition of the mild steel is shown in Table 1. The methods used to prepare specimens for immersion tests and electrochemical measurements are shown in Fig. 1. The sheets were cut into pieces of 7 x 7 mm in size, and a Pb-free solder wire was connected to each specimen for electrochemical measurements. All of the specimens were moulded in epoxy resin (Struers Ltd., EpoFix Resin). The exposed surface of each moulded specimen was ground with silicon carbide abrasive paper from #400 to #4000 and finally polished by colloidal silica. Before the immersion tests, the specimens were taken out from the epoxy resin. All specimens were ultrasonically cleaned in ethanol and then in highly purified water.

Solutions

Five different salt solutions, 1 mM NaCl (Na_{sol}), 0.5 mM $MgCl_2$ (Mg_{sol}), 0.5 mM $ZnCl_2$ (Zn_{sol}), 0.33 mM $AlCl_3$ (Al_{sol}), and 0.5 mM $ZrCl_2O$ (Zr_{sol}), were used as model fresh water. For electrochemical measurements, 0.5 M H_3BO_3 - 0.05 M $Na_2B_4O_7$ (borate) was added to each solution as a supporting electrolyte, and the main metal cation in the solutions was Na^+. All of the solutions were air-saturated. In this study, Na_{sol} was regarded as a standard solution.

The concentration of chloride ions in each solution was adjusted to 1 mM, the same concentration as that in model fresh water. All chemicals were special grade and obtained from Kanto Chemical Co. Ltd. The hardness of cations, X, is expressed as follows [16]:

$$X = [X^0_M + (\sum I_n)^{1/2}]^2 / 10, \quad (3)$$

where X^0_M is the electronegativity of metal atoms and ΣI_n is the total ionized potential from neutral metal atoms to a given oxidized state, n. X calculated by equation (3) increases in the order of Na^+, Mg^{2+}, Zn^{2+}, Al^{3+}, and Zr^{4+} (Table 2).

Immersion tests

Specimens were immersed in the solutions for 28.8 ks (8 h) and 432 ks (5 d) at 298 K. The bottles were open to the air during immersion tests. Before and after the immersion tests, the surfaces of the specimens were observed by a digital camera (Sony Corporation, NEX-C3) and a scanning electron microscope (SEM, JEOL Ltd., JSL6510-LA). The surface of the specimens after immersion for 8 h was analysed by an XPS (JEOL Ltd., JPS-9200) using an Mg Kα X-ray source. The area analysed by the XPS in the experiments was 1 x 1 mm, and depth profiles were obtained by Ar ion sputtering. The sputtering time was converted to depth by applying a sputtering-rate model assuming a sputtering rate of SiO_2. The surface of each of the specimens after immersion for 5 d was analysed by X-ray diffraction (XRD, Rigaku co. Ltd., RINT2200) using a Cu Kα X-ray source. The pH values of the test solutions before and after immersion tests were measured using a pH meter (Eutech Instruments Pte. Ltd., CyberScan 6000).

Electrochemical measurements

All electrochemical measurements were carried out in a three-electrode cell using a potentiostat (IVIUM TECHNOLOGIES, Compactstat). Before the measurements, the working electrodes were immersed in the solutions for 1.8 ks (0.5 h) at 298 K to measure steady open-circuit potential. A Pt plate of 18 cm^2 and an Ag/AgCl-saturated KCl electrode were used as counter and reference electrodes, respectively. Electrochemical impedance measurements were carried out in the frequency range from 10 kHz to 10 mHz, and a modulation amplitude of 10 mV was used. Reproducible data were obtained in all electrochemical tests. The pH values of the test solutions before and after electrochemical measurements were measured using a pH meter.

Results

Immersion tests

Fig. 2 (a) and (b) shows the appearance of specimens after immersion in Na_{sol}, Mg_{sol}, Zn_{sol}, Al_{sol}, and Zr_{sol} for 28.8 ks (8 h) and 432 ks (5 d), respectively. After immersion for 8 h (Fig. 2 (a)), no brown rust or colour change of the solution was observed in the solutions. Fig. 2 (b) shows that there are many brown corrosion products in Na_{sol} and Mg_{sol}. The amounts of those corrosion products in Zn_{sol}, Al_{sol}, and Zr_{sol} were decreased compared with those in Na_{sol} and Mg_{sol}. Fig. 2 (c) and (d) shows surface images of specimens after immersion in Na_{sol}, Mg_{sol}, Zn_{sol}, Al_{sol}, and Zr_{sol} for 8 h and 5 d, respectively. In Fig. 2 (c), there is no brown rust on the specimens, and indistinctly white products are observed on the whole area of the specimens after immersion in Al_{sol} and Zr_{sol}. These results suggest that intense corrosion did not occur on the mild steel during immersion for 8 h. Fig. 2 (d) shows that there are black

corrosion products on the specimens after immersion in Na_{sol} and Mg_{sol}. The brown corrosion products that can be seen in Fig. 2 (b) fell off the specimens when the specimens were taken out from the bottles because the corrosion products have low degrees of adhesion and toughness. Brown corrosion products can be observed on the specimen after immersion in Zn_{sol}. The specimen after immersion in Al_{sol} had fewer brown corrosion products than those on the specimen after immersion in Zn_{sol}. Red corrosion products covered the entire surface of the specimen that had been immersed in Zr_{sol}. All corrosion products on the specimens after immersion for 5 d fell off when the specimens were subjected to ultrasonic cleaning in highly purified water. There was no corrosion product or crevice corrosion on the back side (bottom side) of the specimens after immersion for 5 d.

Fig. 3 shows surface SEM images of specimens before immersion (a) and after immersion for 5 d in (b) Na_{sol}, (c) Mg_{sol}, (d) Zn_{sol}, (e) Al_{sol}, and (f) Zr_{sol}. The corrosion products on the specimens were removed before SEM observation by immersion in highly purified water and ethanol in an ultrasonic bath. The specimen before immersion has a smooth surface (Fig. 3 (a)). There is clear intergranular corrosion after immersion in Na_{sol}, Mg_{sol}, Zr_{sol}, and corrosion behaviours of the grains are different (Fig. 3 (b), (c), and (f)). The specimen after immersion in Zn_{sol} shows many pits, and the intergranular corrosion is not as obvious at that on specimens after immersion in Na_{sol}, Mg_{sol}, and Zr_{sol} (Fig. 3 (d)). Some pits with no intergranular corrosion are observed on the specimen after immersion in Al_{sol} (Fig. 3 (e)). The absence of intergranular corrosion and the presence of some pits on the specimen indicate that metal oxidation may be supressed by the protective films formed on specimens during immersion tests.

Fig. 4 shows corrosion rates calculated by weight loss after immersion for 5 d as a function of *X*. The density of iron, 7.874 g/cm^3, was used to calculate the corrosion rates [18]. The corrosion rate decreased with increase in *X* for all specimens except for those in Mg^{2+}- or Zr^{4+}-containing solution. From SEM results, clear intergranular corrosion was observed on the specimens after immersion in solutions that have large corrosion rates such as Na_{sol}, Mg_{sol}, and Zr_{sol} in Fig. 4. The intergranular corrosion means that metal oxidation and oxygen reduction occurred under the rust layer that can be seen in Fig. 2 (b), and the rust layer may not block oxygen diffusion to the mild steel in fresh water.

XPS surface analyses of specimens immersed for 8 h were carried out to determine whether hard metal cations were incorporated in the passive films before the intense corrosion occurred, and XPS narrow spectra of the metal cations at different depths showed the positions of metal cations. Fig. 5 shows XPS narrow spectra of metal cations of specimens after immersion for 8 h (Fig. 2 (c)) in (a) Na_{sol}, (b) Mg_{sol}, (c) Zn_{sol}, (d) Al_{sol}, and (e) Zr_{sol} at different depths. There is no Na 1s peak on the specimen after immersion in Na_{sol} (Fig. 5 (a)). Peaks of $Mg(OH)_2$ 2p (49.5 eV) [19] are observed from 0 nm to 15 nm for the specimen after immersion in Mg_{sol}, and peaks of Fe 3p (52.4 eV) [20, 21] are observed from 10 nm to 100 nm (Fig. 5 (b)). In Fig. 5 (e), there are two clear peaks of $Zr(OH)_4$ 3d3/2 (185.3 eV) [22] and $Zr(OH)_4$ 3d5/2 (182.8 eV) [23] at all measured depths of the specimen after immersion in Zr_{sol}. Clear peaks of $Zn(OH)_2$ 2p 3/2 (1021.8 eV) [24] and $Al(OH)_3$ 2p 3/2 (74.3 eV) [25] are observed in XPS spectra (Fig. 5 (d)). The results indicate that hard metal cations form a hydroxide layer (more than 10 nm in thickness) on the mild steel after immersion for 8 h, and the thickness of the hydroxides layer may increase with increase in *X*.

The corrosion products formed on the specimens shown in Fig. 2 (d) were analysed by XRD to determine the crystal structure. Fig. 6 shows XRD patterns of the rust on specimens after immersion for 5 h (Fig. 2 (d)). The results indicate that the rust that formed in all solutions consisted of Fe_3O_4 (Na_{sol}: JCPDS 00-003-0863, Mg_{sol}: JCPDS 01-075-1610, Zn_{sol}: JCPDS 01-086-1353, Al_{sol}: JCPDS 01-075-0033, and Zr_{sol}: JCPDS 00-026-1136) and FeO(OH) (JSPDS 00-003-0251), and metal cations are not detected in the rust. The detected ferrite [JCPDS 00-006-0696] and Fe_3C [JCPDS 01-085-0871] would be derived from the substrate of mild steel.

The pH values of the test solutions before immersion and after immersion for 8 h and 5 d are shown in Table 3. All of the solutions after immersion for 5 d showed a slight increase of pH due to formation of OH^- at the metal surface. Al_{sol} had the second lowest pH of the solutions; however, the corrosion rate of the mild steel in Al_{sol} was slowest as shown in Fig. 4. Furthermore, the corrosion rate of mild steel in Zr_{sol} was the same as that in Na_{sol} and Mg_{sol} despite the fact that Zr_{sol} had the lowest pH. The results suggest that the corrosion rate of the mild steel depends on the difference in protective effects of the protective layers formed during immersion tests rather than on pH.

Immersion tests results suggest that hard metal cations in the solutions would form a hydroxide layer on the mild steel during immersion for 8 h, and some hydroxides may inhibit the corrosion of mild steel. Therefore, the initial corrosion behaviour of the mild steel would be a significant step to clarify the different effects of metal cations on the corrosion rate.

EIS analysis

EIS measurements was carried out to clarify the initial corrosion behaviour of the mild

steel and the effect of metal cations on properties of the protective layer. Fig. 7 shows the results of EIS for (a) Nyquist plots and (b) Bode plots of the mild steel in the solutions after immersion for 30 min, and it can be seen that impedance spectra depend on the kinds of metal cations. The fitted lines calculated by Randle's equivalent circuit model [26-28] are also shown in Fig. 7, and the equivalent circuit model is shown in Fig. 8. This model consists of solution resistance (R_{sol}), charge-transfer resistance of the interfacial corrosion reaction (R_{ct}), and constant phase element (CPE), and the fitted lines correspond to the plots of experimental values. The pH values of the tests solutions before and after EIS are shown in Table 4. None of the solutions after EIS showed a change in pH. There was no formation of rust during EIS measurements.

The values of (a) R_{sol}, (b) R_{ct}, and (c) CPE as a function of *X* are shown in Fig. 9. The values of R_{sol} were not changed by *X* (Fig. 9(a)). R_{ct} increased with increase in *X* except for Mg^{2+}- or Zr^{4+}- containing solution (Fig. 9(b)). CPE decreased with increase in *X* except for Mg^{2+} and Zr^{4+} (Fig. 9(c)). High R_{ct} means that the mild steel has high corrosion resistance.

The results of immersion tests and EIS results (Fig. 4 and Fig. 9) showed that the corrosion rate of the mild steel decreases with increase in *X* except for the specimens immersed in Mg_{sol} and Zr_{sol}. In addition, the correlation coefficients of corrosion rate vs *X*, R_{ct} vs *X*, and CPE vs *X* are -0.34, 0.41 and - 0.41, respectively, and these values are too small to regard R_{ct} and CPE as having close relationships with *X*. Therefore, the hardness of cations, *X*, is not suitable as a corrosion indicator of mild steel. Changes in the corrosion resistance of mild steel caused by incorporated metal cations and a novel indicator that is appropriate for estimating the corrosion rate of mild steel in model fresh water are discussed in the following

section.

Discussion

Changes in corrosion caused by metal cations

The structure of passive films formed on mild steels in neutral media has been reported by many researchers. Iitake et al. [29] found by electron diffraction that the passive films consist of Fe_3O_4 and γ-Fe_2O_3 in neutral solutions. Cohen [30] investigated passive films formed in sodium nitrite, and the diffraction pattern indicated that the outermost layer was γ-Fe_2O_3. Mayne et al. [31, 32] found that γ-Fe_2O_3 is formed on mild steel in various solutions. Thus, it can be considered that the analysed hydroxide layer of metal cations would form on γ-Fe_2O_3, and the difference in interatomic distance between the hydroxides and γ-Fe_2O_3 may change the corrosion resistance. The different corrosion mechanisms of mild steel in fresh water depending on the kind of metal cations are explained below.

The corrosion mechanism of mild steel in fresh water with small *X* metal cations such as Na^+ is shown in Fig. 10. There is no incorporation of Na^+ into the passive films as shown in Fig. 5 (a). Cl^- may penetrate into γ-Fe_2O_3 due to the large electronegativity of Cl^- (Fig. 10 (a)), and its penetration may cause formation of $FeCl_3$ [5-9]. The $FeCl_3$ thus formed dissolves in the solution due to its high degree of solubility (Fig. 10 (b)) [5, 6]. This dissolution of $FeCl_3$ means that localized corrosion is initiated on the mild steel (Fig. 10 (c)). The exposed area of the Fe substrate is dissolved by metal oxidation, and oxygen reduction occurs and then OH^- is generated (Fig. 10 (d)). The cathodic reaction is the rate determining step in this situation.

The results of immersion tests suggest that the hydroxide layer is formed on the mild steel after a short period (8 h) of immersion in solutions that contain hard metal cations, and the protective effect of the hydroxide layer differs depending on the kinds of metal cations. The different protective effects of hydroxides of metal cations can be explained on the basis of molar volume. The molar volume is related to the distance between metal ions and hydroxyl groups. Table 5 shows the molar volumes, *V*, of hydroxides of metal cations used in this study and γ-Fe_2O_3 and the molar volume ratio, Δ*V* (ratio of molar volume between the hydroxide of cations and γ-Fe_2O_3). Molar volume is calculated by following equation:

$$V = M / \rho, \quad (4)$$

where *M* is the molar mass, and ρ is the density of the hydroxides and γ -Fe_2O_3 [18, 33]. Δ*V* is expressed as follows:

$$\Delta V = [V_{Fe2O3} / |V_{cat} - V_{Fe2O3}|] / 10, \quad (5)$$

where V_{cat} is the molar volume of hydroxides of cations, and V_{Fe2O3} is the molar volume of γ-Fe_2O_3. ΔV of $Zn(OH)_2$ and that of $Al(OH)_3$ are larger than those of $Mg(OH)_2$ and $Zr(OH)_4$, which did not inhibit corrosion in this study. For this reason, large Δ*V* means that the hydroxide layer formed on the mild steel has good protection against attack from chloride ions in fresh water.

The corrosion mechanism of mild steel in fresh water with large *X* (hard) metal cations such as Mg^{2+}, Zn^{2+}, Al^{3+}, and Zr^{4+} is shown in Fig. 11. Fig. 11 (a), (b), and (c) show the corrosion inhibitory mechanism of the hydroxides of metal cations that have large Δ*V* such as Zn^{2+} and Al^{3+}. The hard metal cations in the solution easily bond with the passive films (Fig. 11 (a)), and the metal cations are incorporated in the passive films and then hydroxides of

metal cations are formed (Fig. 11 (b)). This hydroxides of metal cations may protect the mild steel from chloride ions due to large ΔV of the hydroxides. The surface of the mild steel would not be completely covered by the hydroxide layer because of the model fresh water is a dilute solution; however, the hydroxides layer would prevent the cathodic reaction (Fig. 11 (c)). For this reason, the corrosion rates of the mild steel immersed in Zn_{sol} and Al_{sol} were lower than those in other solutions for a long period.

Fig. 11 (a), (d), and (e) show the corrosion mechanism of mild steel in a solution containing metal cations that have small ΔV such as Mg^{2+} and Zr^{4+}. In the case of mild steel immersed in Mg_{sol}, internal stress may be generated at the $Mg(OH)_2$ / γ-Fe_2O_3 interface, and the stress will cause defects in the hydroxides and the interface (Fig .11 (d)). These hydroxide of metal cations may not protect the mild steel from chloride ions due to the small ΔV of these hydroxides. For this reason, the chloride ions and oxygen easily penetrate the hydroxide layer, and corrosion would occur everywhere on the mild steel. (Fig. 11 (e)) The corrosion mechanism in Zr_{sol} would be the same as that in Mg_{sol} because internal stress may also be generated at the $Zr(OH)_4$ / γ-Fe_2O_3 interface.

Novel corrosion indicator of metal cations

The above-described results and discussion indicate that X is not sufficient to estimate the corrosion rate of mild steel in fresh water and that the difference in molar volume between hydroxides of metal cations and γ-Fe_2O_3 would change the corrosion rate of the mild steel. Thus, a novel indicator to estimate the corrosion rate that takes into account both X and ΔV is needed. Large ΔV means that protective films are formed on the mild steel and large X

means that the metal cations are easily incorporated in the passive films. Therefore, the novel indicator “corrosion inhibitory effect of cations, *Y*” is expressed as follows:

$$Y = X \times \Delta V, \quad (6)$$

and the corrosion rate of the mild steel may decrease with increase in *Y*. The *Y* values are shown in Table 5.

Values of (a) corrosion rate, (b) R_{ct}, and (b) CPE as a function of *Y* are shown in Fig. 12. The correlation coefficients of corrosion rate vs *Y*, R_{ct} vs *Y*, and CPE vs *Y* are -0.95, 0.93, and -0.94, respectively, and these values are sufficient to regard as corrosion rate, R_{ct}, and CPE as having close relationships with *Y* (Fig. 12 (a), (b) and (c)). These results indicate that the corrosion rate of mild steel can be estimated by using the corrosion inhibitory effects of cations, *Y*.

Conclusions

The effects of metal cations on corrosion of mild steel in model fresh water were investigated by surface observation and analysis and by EIS.

1 The corrosion rate of mild steel decreased with increase in the hardness of cations, *X*, in model fresh water except for solutions containing Mg^{2+} and Zr^{2+}.

2 XPS analysis showed that hard metal cations are incorporated in the passive films of the mild steel, and hydroxides of metal cations were formed on the mild steel after immersion for a short time.

3 Hydroxides of metal cations that have large ΔV protect the passive films of mild steel from penetration by chloride ions.

4 The corrosion rate of mild steel can be estimated by using “corrosion inhibitory effect of cations, *Y*”.

Acknowledgments

This study was supported by Hokkaido University Clark Memorial Foundation and by the Salt Science Research Foundation and was conducted at Laboratory of XPS analysis, Hokkaido University, supported by "Nanotechnology Platform" Program of the Ministry of Education, Culture, Sports, Science and Technology (MEXT), Japan.

References

[1] R. E. Melchers, Modelling immersion corrosion of structural steels in natural fresh and brackish waters, Corros. Sci., 48 (2006) 4174-4201

[2] G. S. Vasyliev, The influence of flow rate on corrosion of mild steel in hot tap water, Corros. Sci., 98 (2015) 33-39

[3] M. Itagaki, Y. Yamada, K. Watanabe, T. Nukaga, F. Umemura, Measurement of I-E Curve of Carbon Steel in Fresh Water, Zairyo-to-Kankyo, 53 (2004) 88-94

[4] M. Kato, Corrosion Inhibitors for Iron in Fresh Water, Boshoku Gijutsu, 29 (1980) 89-97

[5] H. J. Engell, N. D. Stolica, Untersuchungen über Lochfraß an passiven Elektroden aus unlegiertem Stahl in chlorionenhaltiger Schwefelsäure, Arch. Eisenhuttenw., 30 (1959) 239-248

[6] H. J. Engell, Stability and Breakdown Phenomena of Passivating Films, Eletrochimica Acta, 22 (1977) 987-993

[7] K. G. Weil, D. Menzel, Die Einwirkung von Halogenionen auf passives Eisen, Z. Elektrochem., 63 (1959) 669-673

[8] R. T. Foley, Role of the Chloride Ion in Iron Corrosion, Corrosion, 26 2 (1970) 58-70

[9] S. Miyake, Study on the Corrosion of Iron by Electron Diffraction, Sci. Papers Inst. Phys. Chem. Research, 36 (1939) 363-370

[10] N.O. Eddy, in: S.K. Sharma (Ed.), Green corrosion chemistry and engineering: opportunities and challenges, John Wiley & Sons, 2011.

[11] G. S. Vasyliev, The Influence of flow rate on corrosion of mild steel in hot tap water, Corros. Sci., 98 (2015) 33-39

[12] M. Kato, Inhibitive Effect of Aluminium Ion for Iron Corrosion in Water (Japanese), Boshoku Gijutsu, 31 (1982) 27-33

[13] S. Takasaki, Development of Environmentally Acceptable Technology for Cooling Water Treatment, Zairyo-to-Kankyo, 64 (2015) 114-120

[14] G. N. Lewis, Valence and the Structure of Atoms and Molecules, The chemical Catalog Co., New York, 1923

[15] R. G. Pearson, Hard and Soft Acids and Bases, J. Am. Chem. Soc., 85 (1963) 3533-3539

[16] M. Misono, E. Ochiai, Y. Saito, Y. Yoneda, A New Dual Parameter Scale for the Strength of Lewis Acids and Bases with the Evaluation of their Softness, J. Inorg. Nucl. Chem. 29 (1967) 2658-2691

[17] K. Otani, M. Sakairia, R. Sasaki, A. Kaneko, Y. Seki, Effect of metal cations on corrosion behavior and surface film structure of the A3003 aluminum alloy in model tap waters, J. Solid State Electrochem., 18 (2014) 325-332

[18] The Chemical Society of Japan, Handbook of Chemistry Basic edition 2 [Japanese], Maruzen, Tokyo, 2004

[19] D. E. Haycock, M. Kasrai, C. J. Nicholls, D. S. Urch, The electronic structure of magnesium hydroxide (brucite) using X-ray emission, X-ray photoelectron, and auger spectroscopy, J. Chem. Soc., (1978) 1791-1796

[20] D. R. Huntley, S. H. Overbury, D. M. Zehner, J. D. Budai, W. E. Brower, Surface characterization of amorphous and crystallized $Fe_{80}B_{20}$, Appl. Surf. Sci., 27 (1986) 180-198

[21] C. S. Kuivila, J. B. Butt, P. C. Stair, Characterization of surface species on iron synthesis catalysts by X-ray photoelectron spectroscopy, Appl. Surf. Sci., 32 (1988) 99-121

[22] S. Sinha, S. Badrinarayanan, A. P. B. Sinha, Interaction of oxygen with $Zr_{76}Fe_{24}$ metglass: An X-ray photoelectron spectroscopy study, J. Less-Common. Met., 125 (1986) 85–95

[23] R. Breniera, J. Mugnierb, E. Miricac, XPS study of amorphous zirconium oxide films prepared by sol–gel, Appl. Surf. Sci., 143 (1999) 85–91

[24] G. Deroubaix, P. Marcus, X-ray photoelectron spectroscopy analysis of copper and zinc oxides and sulphides, Surf. Interface Anal. 18 (1992) 39-46

[25] J. A. Taylor, An XPS study of the oxidation of AlAs thin films grown by MBE, J. Vac. Sci. Technol., 20 (1982) 751-755

[26] I. Martinez, C. Andrade, Application of EIS to cathodically protected steel: Tests in sodium chloride solution and in chloride contaminated concrete, Corros. Sci., 50 (2008) 2948-2958

[27] A. Popova, M. Christov, A. Vasilev, Inhibitive properties of quaternary ammonium bromides of N-containing heterocycles on acid mild steel corrosion. PartⅡ: EIS results,

Corros. Sci., 49 8 (2007) 3290-3302

[28] D. A. Lopez, S. N. Simison, S. R. de Sanchez, Inhibitors performance in CO_2 corrosion EIS studies on the interaction between their molecular structure and steel microstructure, Corros. Sci., 47 (2005) 735-755

[29] I. Iitaka, S. Miyake, T. Iimori, Examination of Passive Iron by Electron Diffraction, Nature, 139 (1937) 156-156

[30] M. Cohen, An Electron Diffraction Study of Films Formed by Sodium Nitrite Solution on Iron, J. Phys. Chem., 56 (1952) 451-453

[31] J. E. O. Mayne, J. W. Menter, The Mechanism of Inhibition of the Corrosion of Iron by Solutions of Sodium Phosphate, Borate, and Carbone., J. Chem. Soc., (1954) 103-107

[32] J. E. O. Mayne, M. J. Pryor, The Mechanism of Inhibition of Corrosion of Iron by Chromic Acid and Potassium Chromate, J. Chem. Soc., (1949) 1831-1835

[33] The Chemical Society of Japan, Handbook of Chemistry Basic edition 1 [Japanese], Maruzen, Tokyo, 2004

Captions

Table 1 Chemical composition of steel (mass%)

Table 2 Hardness of cations, *X* [16]

Table 3 pH values of solutions used before immersion of specimens (pH_{int}) and 5 d after immersion of specimens (pH_{corr}).

Table 4 pH values of the EIS solutions before EIS (pH_{int}) and after EIS (pH_{EIS}).

Table 5 Molar volume, V [31, 32], molar volume ratio, ΔV, hardness of cations, X, and corrosion inhibitory effect of cations, Y.

Fig. 1 Schematic images of methods used to prepare the specimens for immersion tests and EIS.

Fig. 2 Appearance of specimens after immersion in Na_{sol}, Mg_{sol}, Zn_{sol}, Al_{sol}, and Zr_{sol} (a) for 8 h and (b) for 5 d. Surface images of specimens after immersion in Na_{sol}, Mg_{sol}, Zn_{sol}, Al_{sol}, and Zr_{sol} (c) for 5 h and (d) for 5 d.

Fig. 3 Surface SEM images of specimens before immersion (a) and after immersion for 5 d in (b) Na_{sol}, (c) Mg_{sol}, (d) Zn_{sol}, (e) Al_{sol}, and (f) Zr_{sol}.

Fig. 4 Corrosion rate of the specimen in the solution as a function of *X*.

Fig. 5 XPS narrow spectra at different depths of metal cations in specimens after immersion for 8 h in (a) Na_{sol}, (b) Mg_{sol}, (c) Zn_{sol}, (d) Al_{sol}, and (e) Zr_{sol}.

Fig. 6 XRD patterns of the rust formed on specimens after immersion for 5 d.

Fig. 7 Results of EIS in the solutions. (a) Nyquist plots. (b) Bode plots. (c) Nyquist and (d) Bode fitted lines correspond to the plots of experimental values.

Fig. 8 Equivalent circuit model used to fit EIS results.

Fig. 9 Values of (a) R_{sol}, (b) R_{ct}, and (c) CPE as a function of *X*.

Fig. 10 Corrosion mechanism of the passive film in model fresh water with small *X* metal cations.

Fig. 11 Corrosion mechanism of the passive film in model fresh water with large *X* metal cations such as Mg^{2+}, Zn^{2+}, Al^{3+}, and Zr^{4+}.

Fig. 12 Values of (a) Corrosion rate, (b) R_{ct}, and (c) CPE as a function of *Y*.

Table 1 Chemical composition of steel (mass%)

C	Si	Mn	P	S	Fe
0.02	0.01	0.18	0.015	<0.01	bal.

Table 2 Hardness of cations, *X* [16]

Na^{+}	Mg^{2+}	Zn^{2+}	Al^{3+}	Zr^{4+}
1.01	3.54	4.64	7.94	10.22

Table 3 The pH measurement results of the solution used in immersion tests, before immersion of specimens (pH_{int}), 5d after immersion of specimens (pH_{corr}).

Solutions	pH_{int}	pH_{corr}
Na_{sol}	6.0	6.2
Mg_{sol}	5.7	6.2
Zn_{sol}	6.2	6.3
Al_{sol}	4.6	5.3
Zr_{sol}	3.9	4.6

Table 4 The pH measurement results of the EIS solution, before EIS (pH_{int}), after EIS (pH_{EIS}).

Solutions	pH_{int}	pH_{EIS}
Na_{sol} with borate	7.6	7.6
Mg_{sol} with borate	7.6	7.6
Zn_{sol} with borate	7.6	7.6
Al_{sol} with borate	7.6	7.6
Zr_{sol} with borate	7.6	7.6

Table 5 Molar volume, V [31, 32], molar volume ratio, ΔV, hardness of cations, X, and corrosion inhibitory effect of cations, *Y*.

	NaOH	$Mg(OH)_2$	$Zn(OH)_2$	$Al(OH)_3$	$Zr(OH)_4$	γ-Fe_2O_3
Molar volume, V (cm^3/mol)	18.78	24.71	32.60	32.23	49.01	30.48
Molar volume ratio, ΔV	0.26	0.53	1.43	1.74	0.16	-
	Na^+	Mg^{2+}	Zn^{2+}	Al^{3+}	Zr^{4+}	-
Hardness of caions, *X*	1.01	3.54	4.64	7.94	10.22	-
Corrosion inhibitory effect of cations, *Y*	0.26	1.87	6.65	13.79	1.68	-

Specimen for immersion tests

(top view)

1. Mold in resin

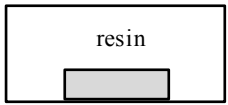

(side view)

2. Polish , take out from resin, ultrasonic cleaning

(top view)

Specimen for EIS

(top view)

1. Connect with a wire

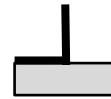

(side view)

2. Mold in resin

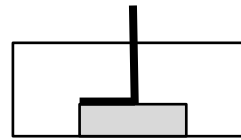

(side view)

3. Polish, ultrasonic cleaning

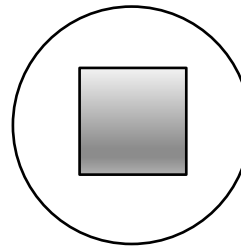

(top view)

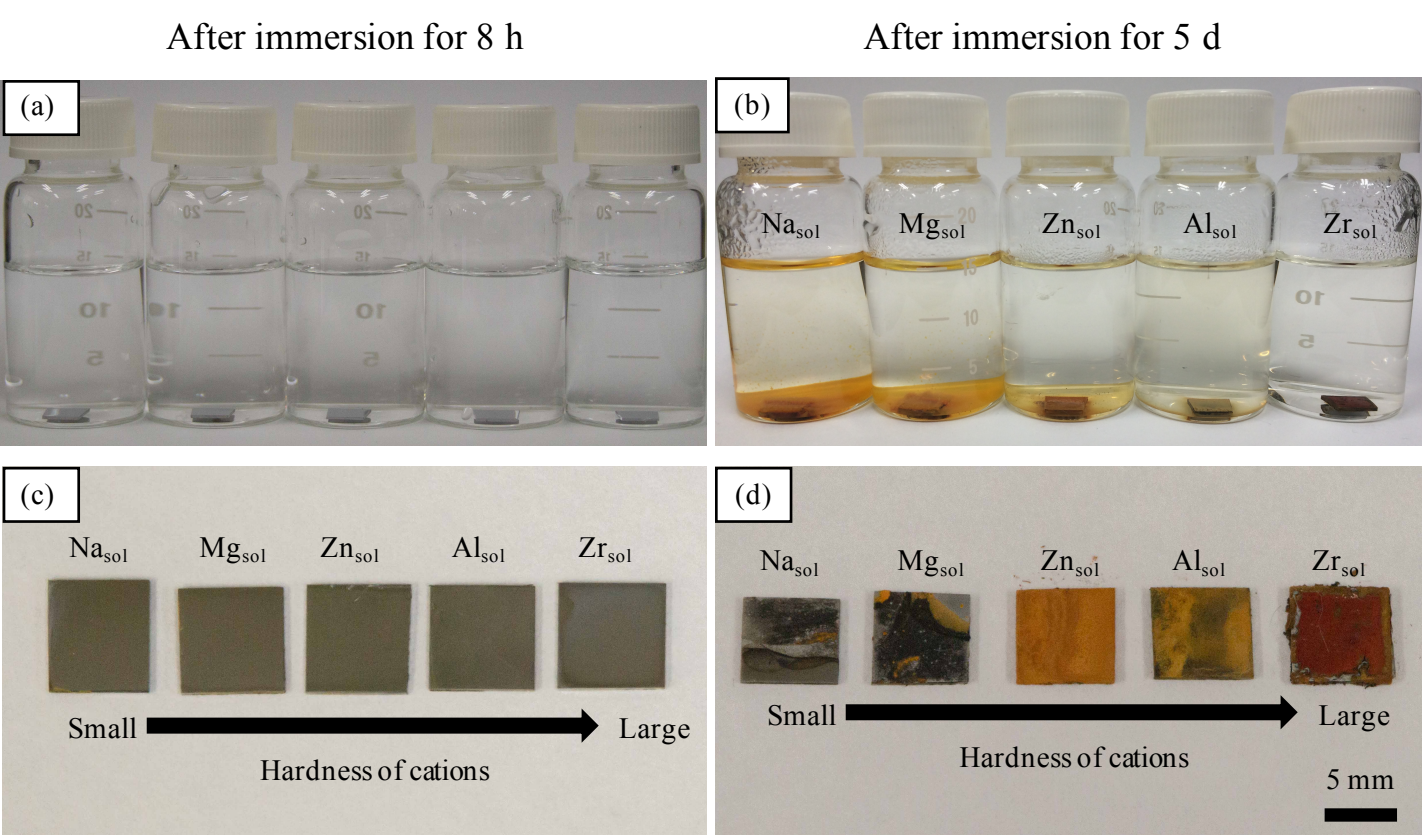
After immersion for 8 h
After immersion for 5 d
(a)
(b)
Na_{sol}
Mg_{sol}
Zn_{sol}
Al_{sol}
Zr_{sol}
(c)
Na_{sol}
Mg_{sol}
Zn_{sol}
Al_{sol}
Zr_{sol}
Small
Large
Hardness of cations
(d)
Na_{sol}
Mg_{sol}
Zn_{sol}
Al_{sol}
Zr_{sol}
Small
Large
Hardness of cations
5 mm

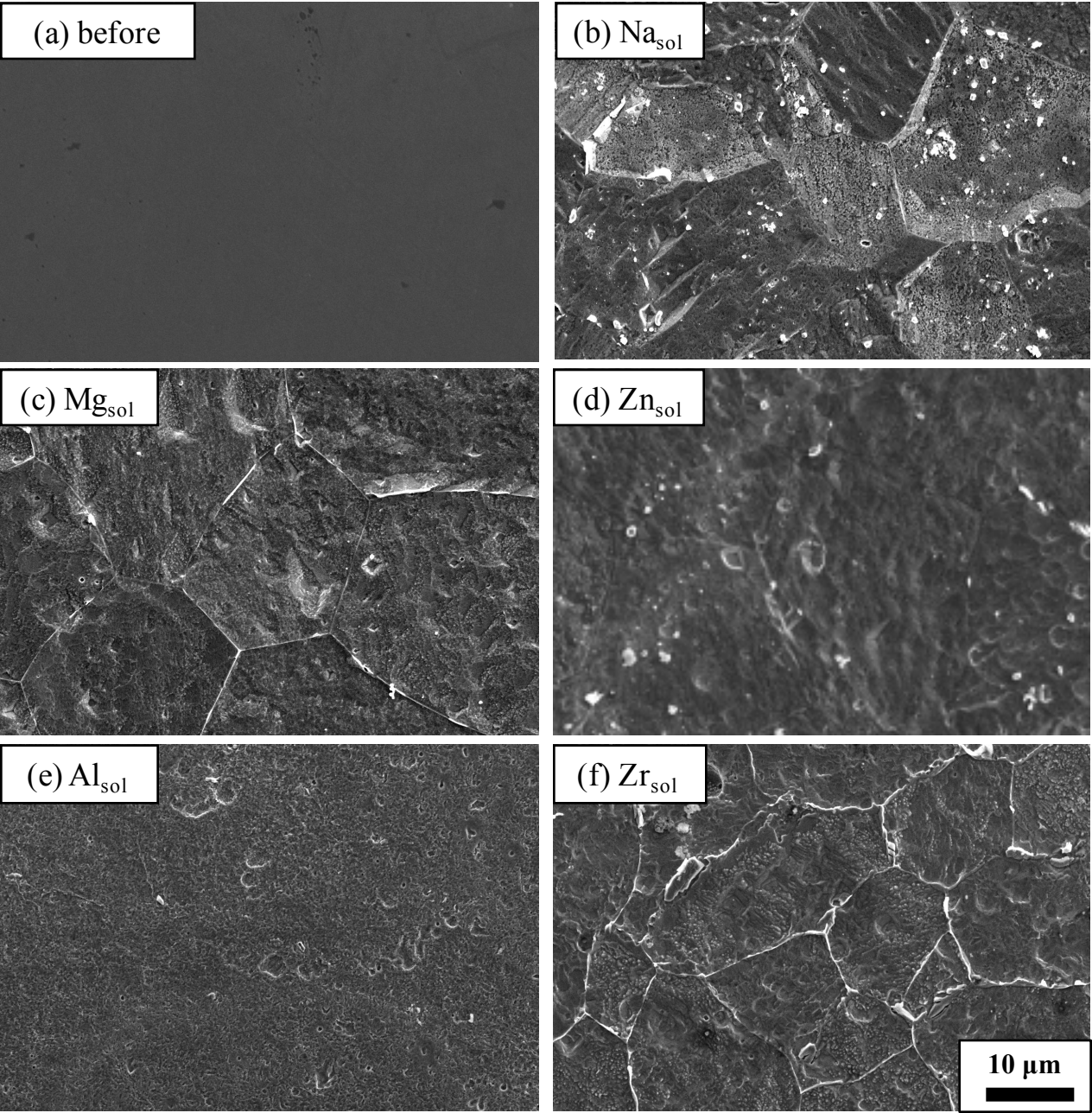
(a) before
(b) Na_{sol}
(c) Mg_{sol}
(d) Zn_{sol}
(e) Al_{sol}
(f) Zr_{sol}
10 μm

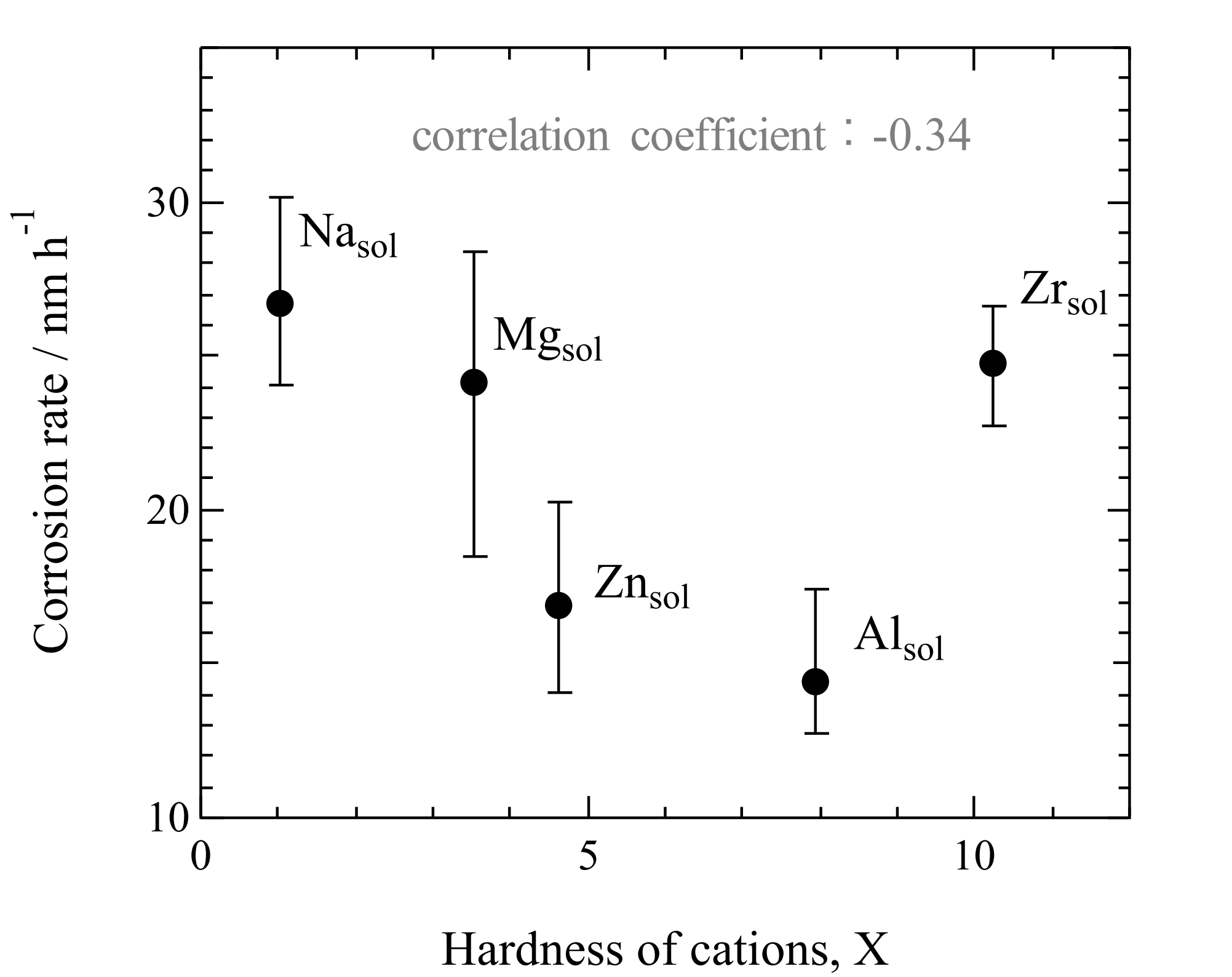
correlation coefficient：-0.34
Na$_{sol}$
Mg$_{sol}$
Zn$_{sol}$
Al$_{sol}$
Zr$_{sol}$
30
20
10
0
5
10
Corrosion rate / nm h^{-1}
Hardness of cations, X

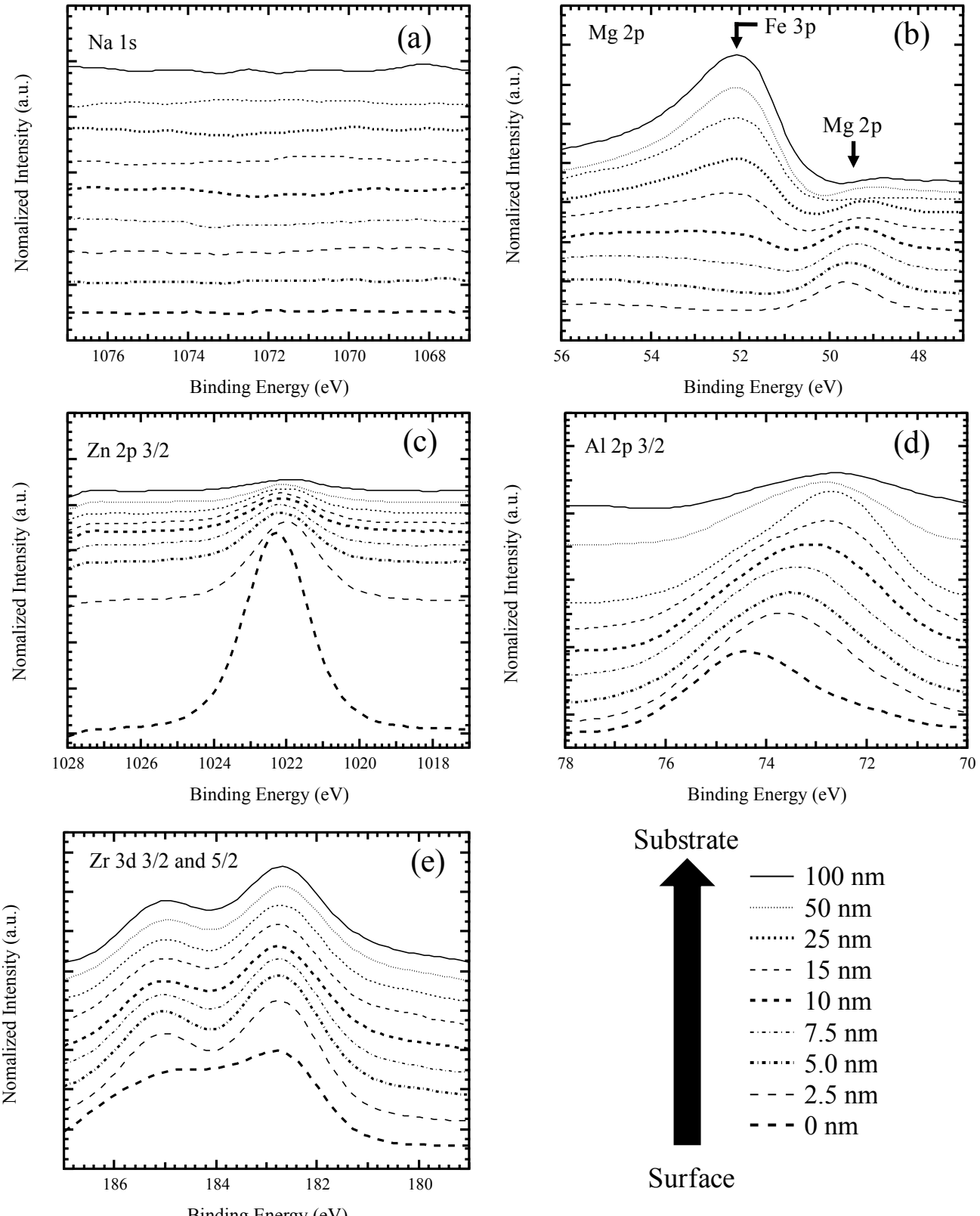
Na 1s
(a)
Nomalized Intensity (a.u.)
1076
1074
1072
1070
1068
Binding Energy (eV)
Mg 2p
Fe 3p
Mg 2p
(b)
Nomalized Intensity (a.u.)
56
54
52
50
48
Binding Energy (eV)
Zn 2p 3/2
(c)
Nomalized Intensity (a.u.)
1028
1026
1024
1022
1020
1018
Binding Energy (eV)
Al 2p 3/2
(d)
Nomalized Intensity (a.u.)
78
76
74
72
70
Binding Energy (eV)
Zr 3d 3/2 and 5/2
(e)
Nomalized Intensity (a.u.)
186
184
182
180
Binding Energy (eV)
Substrate
100 nm
50 nm
25 nm
15 nm
10 nm
7.5 nm
5.0 nm
2.5 nm
0 nm
Surface

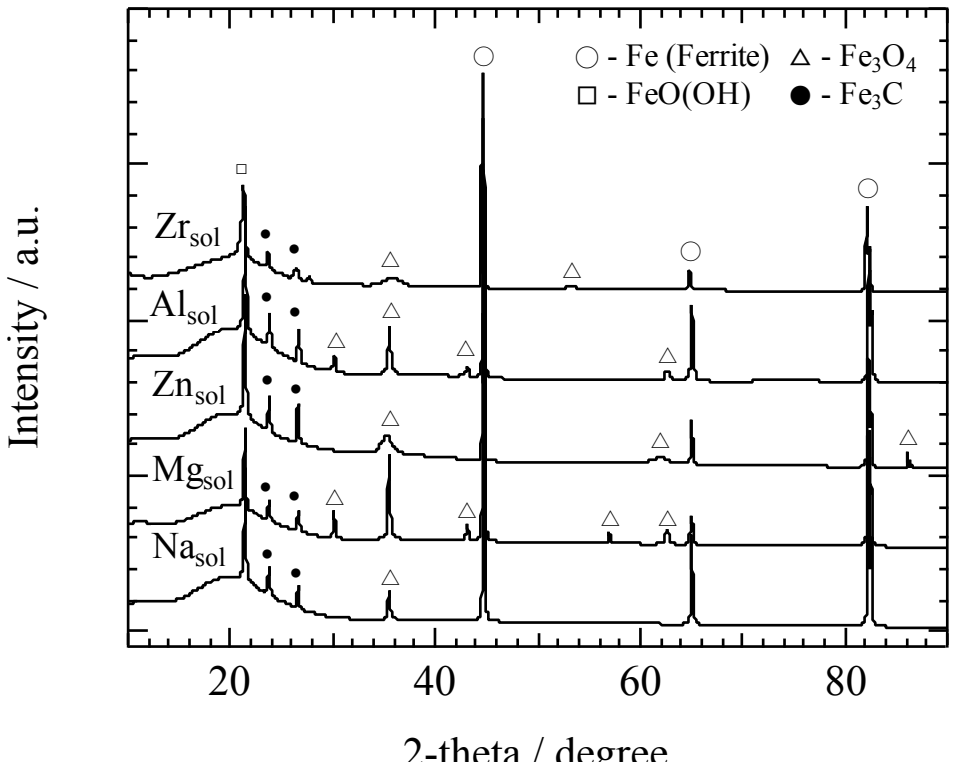
○ - Fe (Ferrite)
△ - Fe_3O_4
□ - FeO(OH)
● - Fe_3C
Zr_{sol}
Al_{sol}
Zn_{sol}
Mg_{sol}
Na_{sol}
Intensity / a.u.
20
40
60
80
2-theta / degree

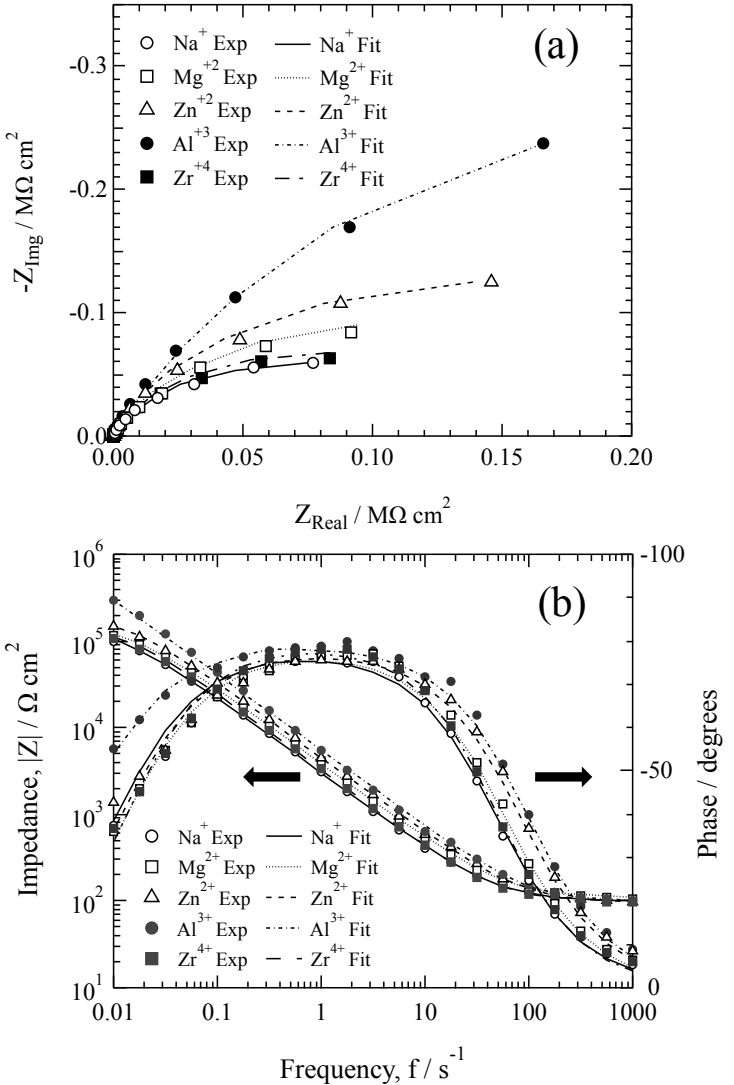
(a)
Na+ Exp
Mg+2 Exp
Zn+2 Exp
Al+3 Exp
Zr+4 Exp
Na+ Fit
Mg2+ Fit
Zn2+ Fit
Al3+ Fit
Zr4+ Fit
-ZImg / MΩ cm2
ZReal / MΩ cm2
(b)
Impedance, |Z| / Ω cm2
Phase / degrees
Frequency, f / s-1

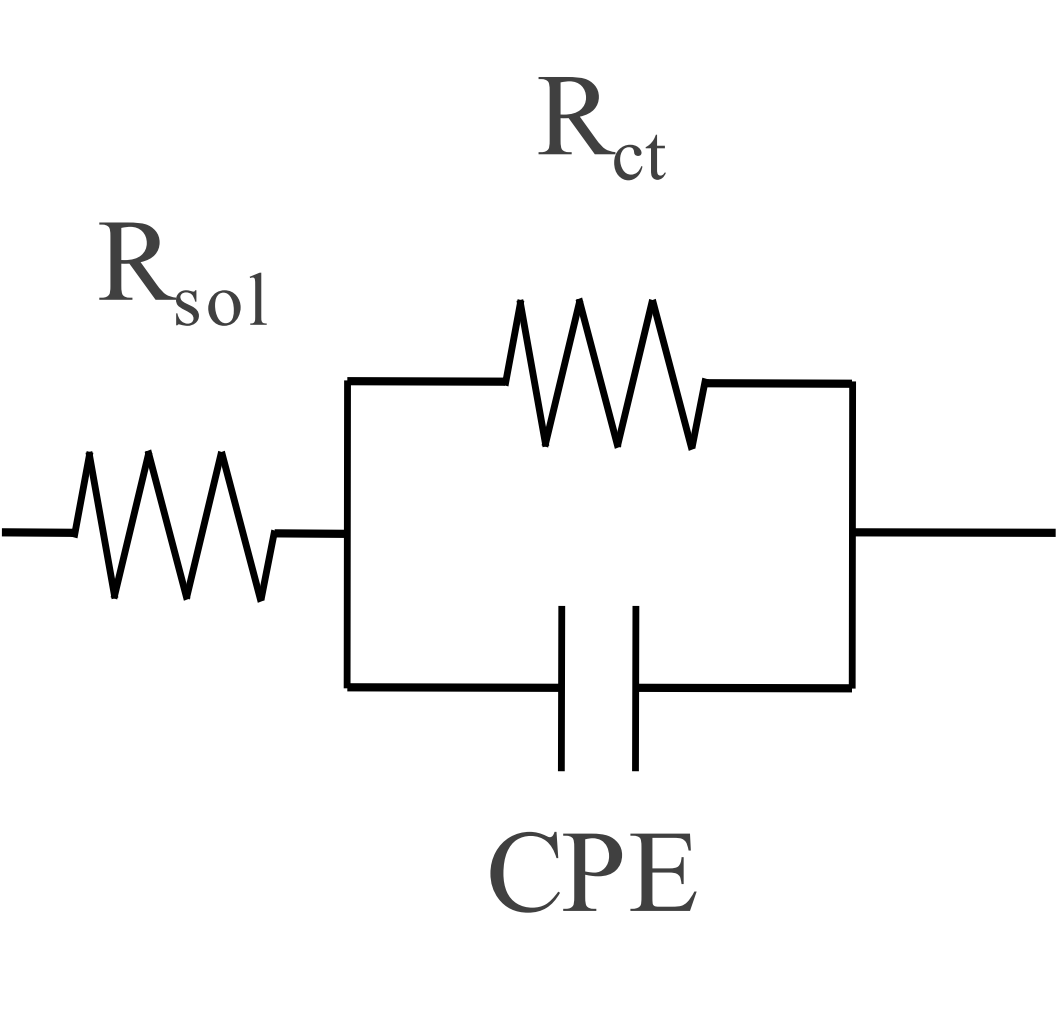
R_{ct}
R_{sol}
CPE

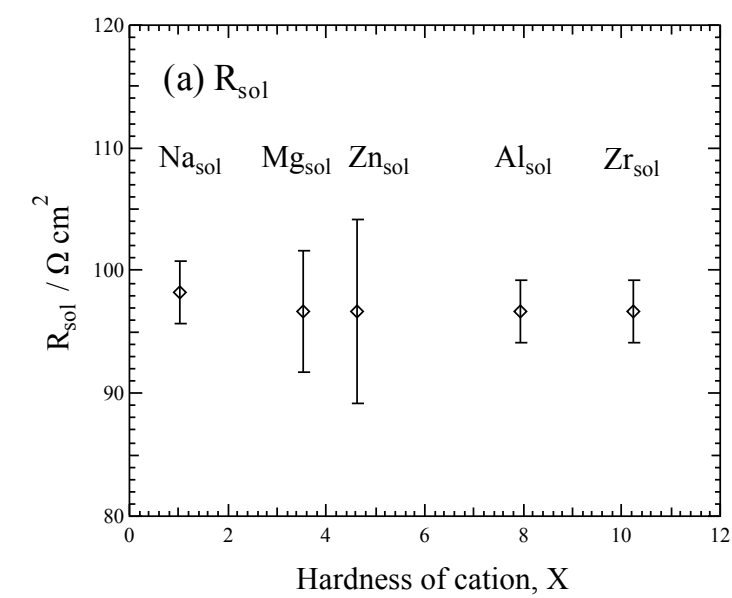
(a) R_{sol}
Na_{sol}
Mg_{sol}
Zn_{sol}
Al_{sol}
Zr_{sol}
R_{sol} / Ω cm^2
Hardness of cation, X

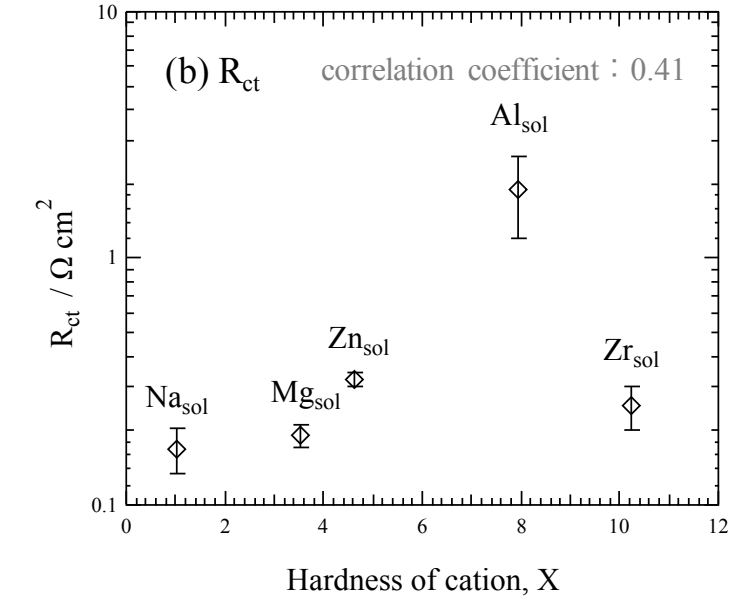
(b) R_{ct}
correlation coefficient : 0.41
Al_{sol}
Zn_{sol}
Zr_{sol}
Na_{sol}
Mg_{sol}
R_{ct} / Ω cm^2
Hardness of cation, X

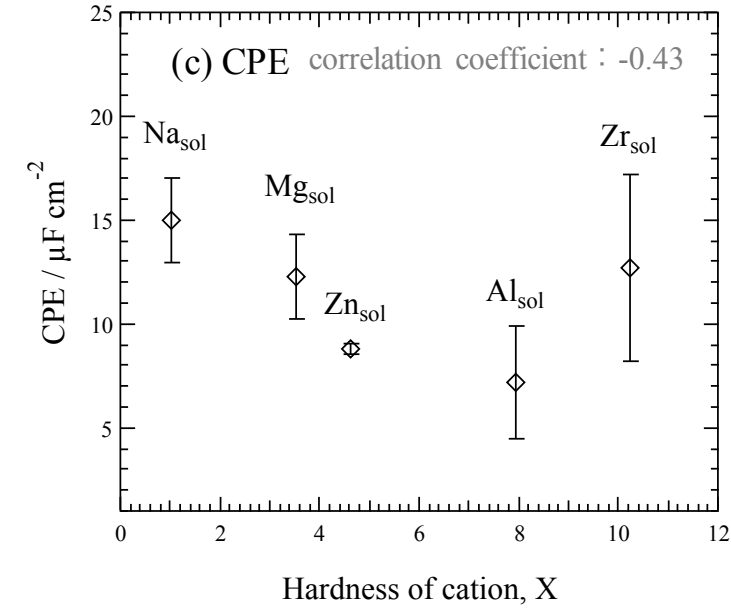
(c) CPE
correlation coefficient : -0.43
Na_{sol}
Mg_{sol}
Zn_{sol}
Al_{sol}
Zr_{sol}
CPE / μF cm^{-2}
Hardness of cation, X

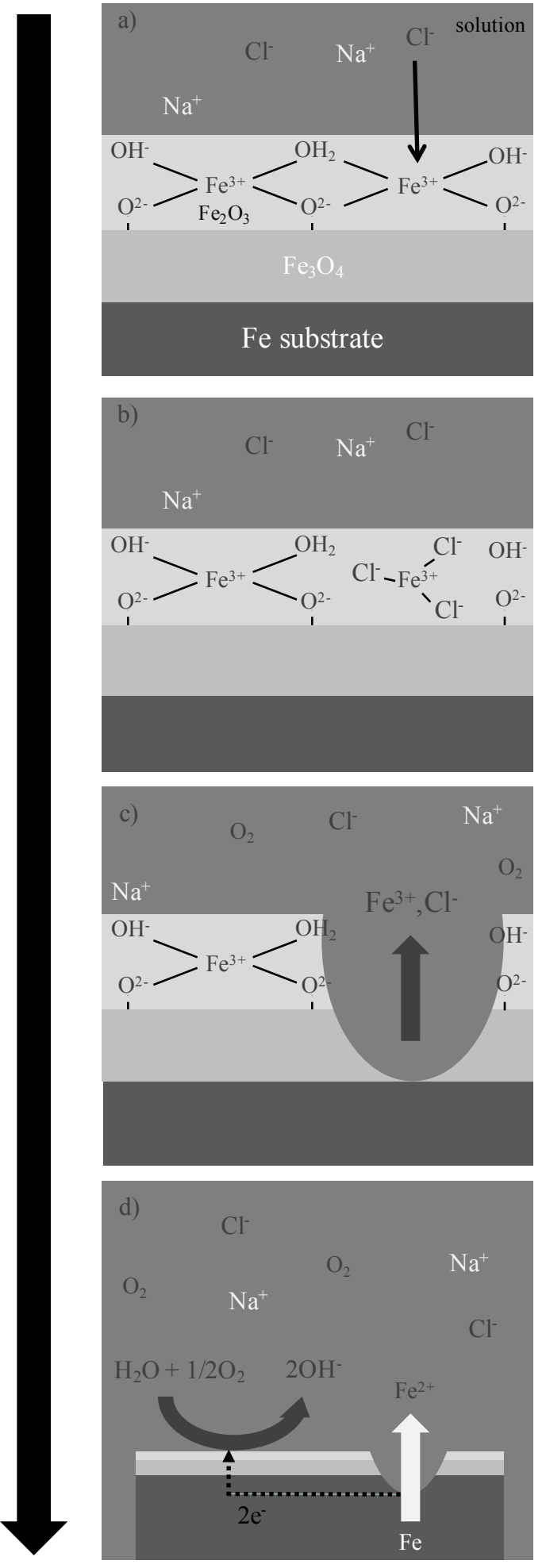
a)
solution
Cl-
Na+
Cl-
Na+
OH-
OH2
OH-
Fe3+
Fe3+
O2-
O2-
O2-
Fe2O3
Fe3O4
Fe substrate
b)
Cl-
Na+
Cl-
Na+
OH-
OH2
Cl-
OH-
Cl-
Fe3+
Fe3+
O2-
O2-
Cl-
O2-
c)
O2
Cl-
Na+
O2
Na+
Fe3+,Cl-
OH-
OH2
OH-
Fe3+
O2-
O2-
O2-
d)
Cl-
O2
Na+
O2
Na+
Cl-
H2O + 1/2O2
2OH-
Fe2+
2e-
Fe

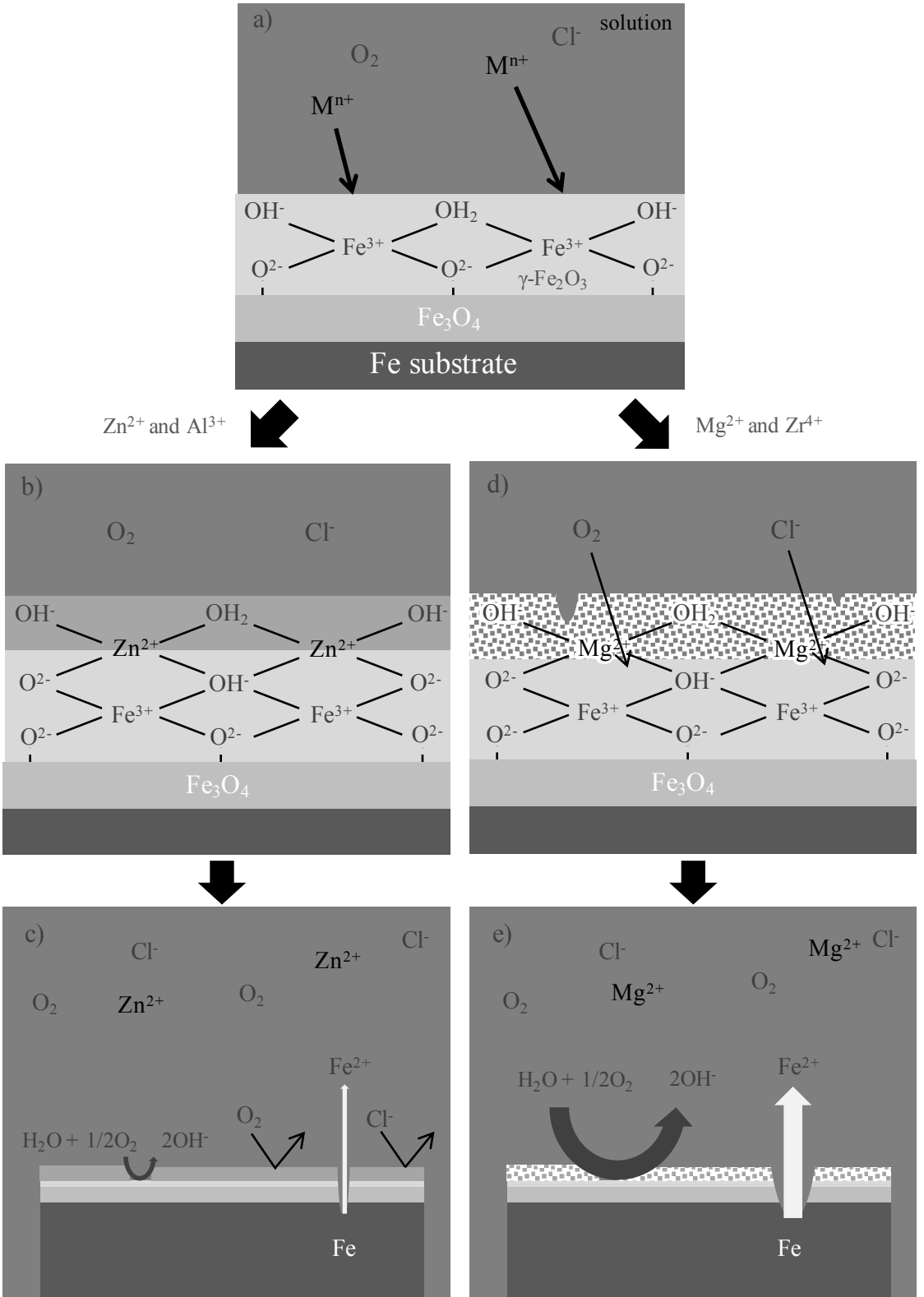
a)
solution
O_2
Cl^-
M^{n+}
M^{n+}
OH^-
OH_2
OH^-
Fe^{3+}
Fe^{3+}
O^{2-}
O^{2-}
O^{2-}
γ-Fe_2O_3
Fe_3O_4
Fe substrate
Zn^{2+} and Al^{3+}
Mg^{2+} and Zr^{4+}
b)
O_2
Cl^-
OH^-
OH_2
OH^-
Zn^{2+}
Zn^{2+}
O^{2-}
OH^-
O^{2-}
Fe^{3+}
Fe^{3+}
O^{2-}
O^{2-}
O^{2-}
Fe_3O_4
d)
O_2
Cl^-
OH^-
OH_2
OH^-
Mg^{2+}
Mg^{2+}
O^{2-}
OH^-
O^{2-}
Fe^{3+}
Fe^{3+}
O^{2-}
O^{2-}
O^{2-}
Fe_3O_4
c)
Cl^-
Cl^-
Zn^{2+}
O_2
Zn^{2+}
O_2
Fe^{2+}
O_2
Cl^-
$H_2O + 1/2O_2$
$2OH^-$
Fe
e)
Cl^-
Mg^{2+}
Cl^-
O_2
Mg^{2+}
O_2
$H_2O + 1/2O_2$
$2OH^-$
Fe^{2+}
Fe

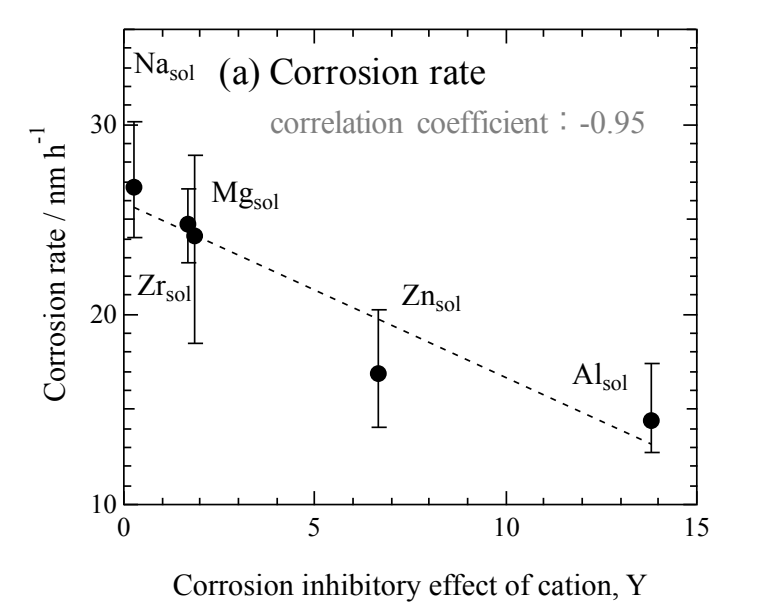
(a) Corrosion rate
correlation coefficient : -0.95
Na$_{sol}$
Mg$_{sol}$
Zr$_{sol}$
Zn$_{sol}$
Al$_{sol}$
Corrosion rate / nm h^{-1}
30
20
10
0
5
10
15
Corrosion inhibitory effect of cation, Y

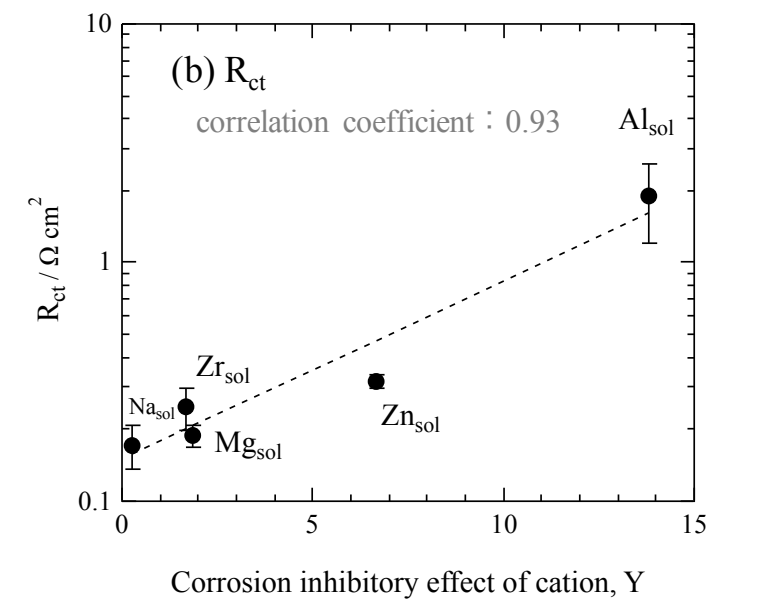
(b) R$_{ct}$
correlation coefficient : 0.93
Al$_{sol}$
Zr$_{sol}$
Na$_{sol}$
Mg$_{sol}$
Zn$_{sol}$
R$_{ct}$ / Ω cm^2
10
1
0.1
0
5
10
15
Corrosion inhibitory effect of cation, Y

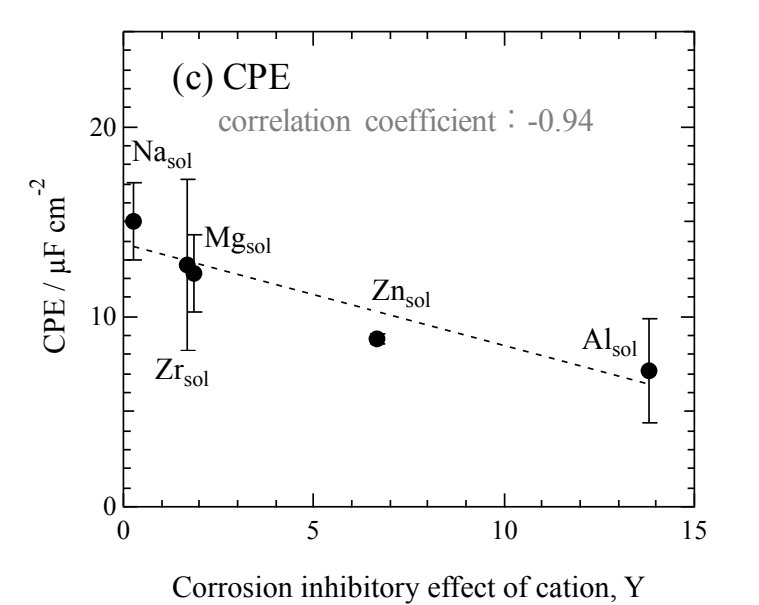
(c) CPE
correlation coefficient : -0.94
Na$_{sol}$
Mg$_{sol}$
Zn$_{sol}$
Al$_{sol}$
Zr$_{sol}$
CPE / μF cm^{-2}
20
10
0
0
5
10
15
Corrosion inhibitory effect of cation, Y